An Audit of Aerodynamic Loss in a Double Entry Turbine under Full and Partial Admission

Peter Newton
peter.newton03@imperial.ac.uk

Colin Copeland
c.copeland@imperial.ac.uk

Ricardo Martinez-Botas*
r.botas@imperial.ac.uk
+44 (0)207 594 47241

Department of Mechanical Engineering,
Imperial College London,
London, UK

Martin Seiler
martin.a.seiler@ch.abb.com

ABB Turbo Systems Ltd.,
Baden, Switzerland

*corresponding author

Abstract

The current study investigates the sources of loss inside a mixed flow, double entry turbocharger turbine under steady inlet conditions in both full and partial admission. Under normal on-engine operation, it is likely that both limbs in a double entry device will be fed by exhaust pulsations which are out of phase meaning that the turbine will spend most or all of the time with unbalanced flow through each limb. In the extreme case one limb will be flowing whilst the other is stagnant, this is the partial admission condition. Even under steady state inlet conditions, unequal admission is an important effect to study on the way to fully understanding pulsed operation of a double entry device.

This paper presents 3D computational analyses of the flow inside a double entry turbine under both full and partial admission. The computational results are compared to experimental results of Copeland (2009) and Copeland *et al* (2010). The distribution of loss within the turbine is evaluated for each computational condition by means of entropy production. In the full admission case the most significant area of loss was found to be in the tip region. Under the partial admission condition the flow regime is very different. In this case the rotor wheel was found to be acting in a fully unsteady manner, with the flow being unable to reach a fully developed state throughout the flowing section of the volute. The most significant area of entropy generation in the partial

admission case was associated with interaction of the flows in each sector of the volute, this occurred in the inter-space between the nozzle exit and the rotor passage inlet.

Keywords

Double-entry, Turbocharger, Turbine, Entropy Production, CFD

1. Introduction

In an exhaust turbocharger system it is desirable to transfer as much of the gas energy from the point of the engine exhaust valve to the turbine wheel as possible, with minimum dissipation. As each cylinder exhausts this leads to a highly unsteady flow driving the turbine wheel, a problem inherent in coupling a roto-dynamic device to a positive displacement one.

A problem with pulse turbocharging is encountered when two or more engine cylinders have overlapping exhaust pulses. Not only can this damp the high energy pressure pulses but more importantly can have an adverse effect on the exhaust manifold wave dynamics. This leads to the dual entry turbine which allows two separate flows to enter the turbine wheel, whilst keeping them isolated as far as possible. Watson and Janota (1982) find that optimal performance is obtained when 3 cylinders, whose firing sequences are evenly spaced (i.e. 240 crank angle degrees on a 4 stroke engine or 120 crank angle degrees on a 2 stroke engine), are connected to each turbine entry. This makes the dual entry turbine ideal for an in-line 6 cylinder engine although they are used under many other configurations. Turbochargers with up to 4 entries to a single turbine wheel can be found on engines with a larger number of cylinders: however, in this case it is more common that 2 dual entry turbochargers would be employed instead. Whichever configuration is used it is important that the manifold is tuned such that the pressure reflections to and from the turbine do not interfere detrimentally with the operation of the engine.

Dual entry turbines are commonly found in two different formations: the *twin-entry* volute, where each entry supplies the whole 360 degrees of the turbine periphery but only half of the span; the *double-entry* volute, where each entry supplies a 180 degree section of the turbine wheel. With any multiple entry turbine fitted to an engine it is likely that, at any point in time, each entry will not be at exactly the same condition of pressure and mass flow rate as the next. This gives rise to an unequal flow condition at the turbine wheel. The extreme case, where one entry is flowing whilst the other entry is stagnant, is referred to as the *partial* admission condition. During real world operation a dual entry turbine will spend the majority of its time under some condition of unequal flow through each limb. This suggests that, even though the unequal admission effect can be analysed in a

steady manner, this is an important feature to study in order to begin to understand the fully unsteady performance of a multiple entry turbocharger turbine. This may not only be a consideration for the turbine designers, where current methodology is to design for full admission performance, but this can also help in turbocharger-engine matching and simulation. Here again it is commonplace to base the turbocharger performance upon the full admission performance of the turbine without considering the partial and unequal operation, which, in the extreme case can differ significantly to the equivalent full admission condition. Copeland (2009), showed how to use the steady partial and unequal admission turbine performance to obtain a full quasi-steady analysis of a turbine acting under pulsed operation. The current study deals with the flow inside a double entry device, shown in Figure 1.

In the past two decades most of the research concerning dual entry turbocharger turbines has looked at the twin entry turbine with the exception of Copeland *et al*. (Copeland *et al.* 2008, 2009, 2010; Copeland 2009) who carried out an extensive research programme assessing the performance of a double entry turbine in both steady and unsteady conditions. All other published research regarding the double entry turbine was carried out before 1980 (Benson 1974; Benson and Scrimshaw 1965; Mizumachi *et al.* 1979; Pischinger and Wunsche 1977; Wallace and Blair 1965; Wallace *et al.* 1969; Wallace and Miles 1970). In steady testing Copeland *et al*. (Copeland *et al*. 2008, 2009, 2010; Copeland 2009) find a considerable decline in performance when the turbine is operated in unequal admission, this corroborates with previous researchers. In the extreme, partial admission condition, the performance deficit was found to be upwards of 30 percentage points in turbine efficiency. In the most recent publication of Copeland *et al.* (2010) an effort was made to explain some of their experimental findings on unequal admission using a computational analysis of the whole turbine system. Although some understanding of the partial admission flow was gained from this analysis, the model was not considered refined enough to justify a more detailed investigation of the flow field.

As far as the authors are aware the previous study by Copeland *et al.* (2010) is the only published 3D computational analysis of a double entry turbine. The current study aims to carry out a more refined computational analysis to assess the main areas of loss in a double entry turbine in both full and partial admission and hence gain a deeper understanding of the differences between the two flow regimes.

2. Entropy production

The main aim of this paper is to show the division of losses inside the turbine and to explore how this changes when the turbine is operated in a condition of partial admission. Traditionally the different losses are

classified by a series of total pressure loss coefficients. These have been used in the past simply because they are easy to calculate from cascade data although, as Denton (1993) points out, this does not necessarily mean that this is the most convenient form. He concludes that the most rational measure of loss generation in an adiabatic machine is in entropy creation. Entropy is a useful concept in the design of fluid machinery where, in an adiabatic device, the creation of entropy relates directly to the destruction of useful work and hence to a loss in efficiency.

The use of entropy generation rate is particularly advantageous in a Computational Fluid Dynamics (CFD) simulation where point wise entropy generation can be calculated directly, demonstrated by several researchers (Copeland *et al*. 2010; Kock & Herwig 2005; Moore & Moore 1983a, 1983b; Pullan *et al*. 2005; Sciubba 1997). Sciubba (1997) outlines the superiority of this method over traditional loss correlations for identifying regions of loss inside a turbo machine. Perhaps more pertinent to the current investigation Pullan *et al* (2005) used the method of entropy generation rate to show different areas of loss inside a turbine passage. Copeland *et al*. (2010) also used the idea of entropy generation rate to demonstrate areas of loss generation in a double entry turbine system.

Greitzer *et al* (2004) derive an analytical expression for the entropy production rate per unit mass in a fluid system;

$$\frac{Ds}{Dt} = \frac{\dot{Q}}{T} - \frac{1}{\rho T}\frac{\partial q_i}{\partial x_i} + \frac{\tau_{ij}}{\rho T}\frac{\partial u_i}{\partial x_j} \qquad (1)$$

The first term on the right hand side of Equation 1 represents the change in entropy of the system due to an internal heat source, such as combustion, with a heat rate $\dot{Q}$, this term can be ignored in the current analysis. The second term represents the entropy change due to heat flux, where q_i is the *ith* component of the heat flux vector, $\boldsymbol{q}$. This may be modeled as the product of thermal conductivity and the temperature gradient:

$$q_i = k\frac{\partial T}{\partial x_i} \qquad (2)$$

The final term on the right hand side represents the dissipation of mechanical energy into entropy where τ_{ij} is the viscous stress tensor:

$$\tau_{ij} = \mu\left(\frac{\partial u_i}{\partial x_j} + \frac{\partial u_j}{\partial x_i}\right) + \delta_{ij}\lambda\nabla \cdot u \qquad (3)$$

In order to implement Equation 1 directly, in a turbulent flow, the time and length scales of the very smallest eddies would have to be modeled explicitly (a Direct Numerical Simulation), which would be highly impractical and require very large computing times. In reality the effects of these very small turbulent eddies are accounted for in the turbulence model. Moore and Moore (1983a) extended this analytical equation for application with an eddy viscosity turbulence model. In their analysis they neglect the effect of internal heating sources and first develop an expression for entropy generation per unit volume, applying the Reynolds decomposition for temperature and velocity:

$$\bar{T}\sigma = \frac{k}{\bar{T}}\left[\left(\frac{\partial \bar{T}}{\partial x_i}\right)^2 + \overline{\left(\frac{\partial T\prime}{\partial x_\iota}\right)^2}\right] + \bar{\tau}_{ij}\frac{\partial \overline{u_\iota}}{\partial x_j} + \overline{\tau'_{\iota J}\frac{\partial u_\iota\prime}{\partial x_J}} \qquad (4)$$

For the current model, the system was adiabatic and the effect of thermal diffusion was assumed to be negligible compared to the generation of entropy through turbulent viscous dissipation. This allowed the entropy generation term associated with heat flux on the right hand side of Equation 4 to be neglected. Finally, Moore and Moore (1983a) use the eddy viscosity to model the turbulent viscous dissipation:

$$\overline{\tau'_{\iota J}\frac{\partial u_\iota\prime}{\partial x_J}} = \frac{\mu_t}{\mu}\bar{\tau}_{ij}\frac{\partial \overline{u_\iota}}{\partial x_j} \qquad (5)$$

The equation for entropy generation rate per unit volume, used in this study, is finally given by;

$$\sigma = \frac{1}{\bar{T}}\left(\bar{\tau}_{ij}\frac{\partial \overline{u_\iota}}{\partial x_j} + \frac{\mu_t}{\mu}\bar{\tau}_{ij}\frac{\partial \overline{u_\iota}}{\partial x_j}\right) \qquad (6)$$

All variables in Equation 6 can be readily obtained in most standard CFD packages. This quantity can be integrated over a control volume in order to evaluate the instantaneous entropy production.

3. Computational Analysis

The computational analyses were run using the 3D, viscous, Navier-Stokes solver *Ansys CFX 12.1*. This is a general purpose, commercial CFD code although the pre- and post processors contain many functions specifically intended for the analysis of turbomachines, which lends it particularly to the current application.

The computational analyses were separated into two distinct parts: Single passage analyses were used to simulate the full admission condition; a full turbine model was required to model the partial admission condition.

3.1 Mesh Sensitivity

In order to test the sensitivity to of the predicted flow field to mesh refinement, five different grids were tested for the turbine rotor domain, ranging between 15,000 elements and 1.8 million elements per passage. In prediction of turbine performance, mesh density had negligible effect as both mass flow and efficiency were predicted similarly by all the different meshes. A comparison of the predicted and measured turbine performance is given in the Section 4.1 for the final mesh. Although a good prediction of the turbine performance is encouraging, this does not necessarily guarantee a good prediction of the flow field.

The flow prediction by each mesh was further analysed by examination of the velocity field downstream of the trailing edge of the rotor blade. This was done mainly in a qualitative sense, by looking at contours of velocity. It was clear that the lower density meshes, below 100,000 elements per rotor passage, were unable to resolve some of the more detailed aspects of the flow which were predicted by the higher density meshes, even though the overall performance prediction was very similar. Beyond a rotor mesh density of around 400,000 elements per rotor passage the prediction of various details in the trailing edge velocity field was more consistent and almost no change was observed in the predicted flow field when the mesh density was increased beyond 950,000 elements per rotor passage, although this does not necessarily guarantee a grid independent solution. The final mesh chosen contained 990,000 nodes per rotor passage and was composed entirely of hexahedral elements. Each nozzle passage was also composed fully of hexahedral elements and contained 100,000 nodes. The choice of mesh was made based on both the mesh sensitivity analysis and a practical limit on the maximum grid size for the computational resources available, since the same mesh was used in both the full admission (single passage) analyses and the partial admission analysis which necessitated modelling of the whole turbine system including 12 rotor passages and 24 nozzle passages and the full volute and exit duct.

The computations were run on the high performance computer (HPC) at Imperial College: this is a centrally based PC cluster allowing vast parallel computations. The partial admission case, which consisted of over 14 million mesh nodes in total, was run on 3 HPC nodes, each with 8 CPUs and a RAM availability of 16GB. Even with this capacity computation times for this case were on the order of a week in total in order to model two complete rotations of the turbine wheel.

3.2 Full Admission Analysis

In order to model the full admission condition, rotational periodicity was exploited so that a single turbine passage could be used to model the whole geometry: this allows a significant saving of computational effort. The flow domain consisted of a 30 degree sector containing two nozzle passages and a single rotor passage. An inlet block was added upstream of the nozzle domain and an exit duct downstream of the rotor passage in order to allow full development of the pressure and velocity fields.

In a single passage model it is important to model the inlet boundary conditions correctly: the direction of the flow at the inlet to the nozzle must emulate the conditions at the exit to the volute, which is not modelled explicitly. A free vortex flow was assumed, with a swirl coefficient of 0.9, as proposed by Japikse and Baines (1994), in order to specify the flow direction. Using experimental data the flow velocity at the entrance to the volute was calculated, the meridional velocity component was evaluated by assuming a constant mass flow into the rotor wheel around the periphery of the volute. Table 1 outlines the settings for the single passage model.

3.3 Partial Admission

Unequal admission in a double entry turbine creates an unsteady effect within each turbine passage as the wheel rotates between the two sectors of the volute, which are at different pressures. Since this is an important effect to model, adopting a single passage analysis would not be acceptable to capture this behaviour. Perhaps the greatest discrepancy would be in the assumption that the flow in each passage would be exactly the same. It was also apparent from the work of Copeland *et al*. (2010) that the peripheral flow around the rotor wheel contributes significantly to the behaviour of the turbine as a whole under partial admission. Considering this a model of the turbine system was constructed incorporating the full volute, 24 nozzle passages, 12 rotor passages and an exit duct, this is shown in Figure 2.

To capture the unsteady effect in each rotor passage a transient simulation was carried out. A transient rotor-stator interface was applied such that the rotor was explicitly rotated by 1 degree per time step so that each rotor pitch was traversed by 30 individual time steps. This was small enough that the solution converged within 10 iterations to an RMS residual value of 10e-05 in each time step. Two full rotations of the turbine wheel were modelled, which corresponded to 720 individual time steps, this allowed the solution to reach periodic convergence. The parameters for the partial admission case are outlined in Table 2.

3.4 Division of the Passage

Losses in a turbomachine are traditionally classified into different areas such as tip leakage loss, windage loss, secondary flow loss etc. As many authors have outlined before (Baines *et al*. 2003; Denton 1993), on a real turbomachine the division between each of these types of loss becomes blurred and it is impossible to determine whether a particular area of loss should be attributed to one or the other. Because of this, the division of the passage into different areas of loss generation was somewhat arbitrary although some thought was given to the fluid dynamic processes within the rotor blade passage. The stator domain was taken as a single control volume whilst the rotor blade domain was divided into 7 further volumes.

Figure 3A shows the division of the rotor blade passage from a blade to blade perspective. The *Interspace* area consisted of everything between the exit of the stator domain and the leading edge of the rotor blade. The *Pressure Side* (PS), *Suction Side* (SS) and *Exit* areas were further divided into *Tip* and *Passage* sections. The *Tip* area included everything above 75% of blade span, this was found to incorporate the majority of the tip leakage vortex for most cases and the *Passage* area included everything below this. This can be seen in Figure 3B which shows the division of the passage in a meridional orientation.

4. Results

4.1 Single passage

4.1.1 Comparison with experimental data

The single passage analysis was conducted at 90% of design speed, which corresponded to a shaft speed of 52,000 rpm. The pressure ratio ranged between 1.3 and 3, which equated to velocity ratios between 1.05 and 0.53 respectively. The computational results were compared to the full admission experimental results of Copeland (2009) for both Pressure Ratio against Mass Flow Rate and Efficiency against Velocity Ratio. The comparisons are shown in Figure 4 and Figure 5. In these figures the mass flow rate and efficiency figures have been normalised by the corresponding values for the experimental peak efficiency case.

Below an isentropic velocity ratio of around 0.85 the computational analysis predicts the efficiency of the turbine to be generally higher than the experimental case. This discrepancy is around 5 percent for the peak efficiency point. At values of velocity ratio higher than this, the CFD model predicts a sharper deterioration in efficiency than is seen in the experimental data, this effect was also seen in the analysis by Copeland et al. (2010). At a velocity ratio of 1.05 the CFD analysis under predicts the experimentally measured efficiency by around 10 percent, this does however correspond to an area of steep decline in efficiency with isentropic

velocity ratio. Overall the prediction of turbine efficiency by the CFD model shows a satisfactory agreement with the experimental data, especially at lower values of velocity ratio.

It is worth noting that the largest discrepancies between the experimental and computational results are seen in the lower power region of the turbine performance line, this is the area of greatest uncertainty in the experimental results which can be as high as ±5% in terms of normalised efficiency (Copeland 2009). Some discrepancy between the computational and experimental results would be expected however, due to simplifications inherent in the CFD model. Perhaps the largest simplification in the computational analysis is that the single passage model does not account for the volute and any loss associated with it. In addition, the CFD analysis does not model the windage losses on the back face of the rotor and it assumes an aerodynamically smooth surface for all solid boundaries, on the actual turbine there are tool paths caused by the manufacture of the turbine wheel. It is also clear that the CFD model is based on approximations of fluid behaviour, the most significant being the turbulence model. Although the k-ε model used here is one of the most prominent and well validated turbulence models it is evident that it will not predict the turbulent effects fully in all flow situations.

The predicted mass flow characteristic follows the experimental data very well. At the lowest pressure ratio there is roughly a 3 percent discrepancy, whilst at the higher pressure ratio this is less than 1 percent.

4.1.2 Distribution of losses

Figure 6 shows the distribution of normalised entropy generation per unit shaft work against velocity ratio for the single passage computational analysis. The normalisation value was taken as the entropy generation rate per unit shaft work within the rotor and stator in the peak efficiency case. At peak efficiency (Operating point A in Figure 6, velocity ratio 0.63, pressure ratio 2.1) the losses within the turbine are dominated by tip effects (*SS Tip, PS Tip* and *Exit tip*) with the largest contribution coming from the tip section on the suction side (*SS Tip*). At this operating condition the incidence angle entering the rotor passage is about -12 degrees. This is a favourable degree of incidence and results in a fairly orderly flow field that follows the blade curvature on both the Pressure and Suction Sides of the blade. A strong tip leakage vortex is evident on the suction side of the blade leading to higher losses in this area. In the lowest velocity ratio case (Operating point B in Figure 6, velocity ratio 0.53, pressure ratio 3.0) the distribution of losses remains similar to those at peak efficiency apart from a noticeable increase in losses in the *SS Passage* section. This is due to a slightly positive incidence angle

(+11 degrees) as the flow impinges on the leading edge of the blade. This leads to a separation of the flow on the suction side of the leading edge of the blade, leading to increased losses in this area. At the highest velocity ratio (Operating point C in Figure 6, velocity ratio 1.05, pressure ratio 1.3) the losses are distributed quite differently to the peak efficiency case (Operating point A in Figure 6). In this case the incidence angle is -72 degrees: this represents a highly adverse condition. The flow here impinges on the suction surface of the blade and accelerates around the leading edge causing a large region of separation on the pressure surface of the blade and very large associated losses throughout the passage: this tends to dominate the flow through the rest of the blade passage.

4.2 Partial Admission

4.2.1 Comparison with Experimental Data

The Computational analysis of the partial admission case was carried out with exactly the same conditions as measured by experiment. The inlet total pressure to the inner (flowing) limb was 199537Pa with a total temperature of 320.7K. The exit static pressure was 100783Pa and the turbine speed 49431rpm. This corresponds to a velocity ratio of 0.657 and pressure ratio of 1.97 across the flowing limb.

Figure 7 & Figure 8 show a comparison between the current CFD analysis, the experimental data and the previous computational analysis of Copeland *et al* (2010) for efficiency and effective area respectively. The effective area is the hypothetical throat area which would be needed to pass the turbine mass flow if a nozzle was acting isentropically over the same pressure ratio as the turbine. This parameter shows the turbine swallowing capacity and was used by Copeland *et al* in plots of unequal admission instead of mass flow. The abscissa on both of these figures shows the ratio of pressures between the two entries in the double entry turbine. A value of unity represents the full admission condition and as this value moves away from unity the turbine experiences a higher degree of unequal admission. It is worth noting that Figure 8 represents only the effective area of the inner (flowing) limb. In the experimental results and the previous CFD results of Copeland *et al* (2010) the pressure ratio across this limb was held constant at approximately 2.0 whilst the pressure ratio in the outer limb was varied to observe the effect of different degrees of unequal admission, in the partial admission case the outer limb was closed such that no mass was able to flow through it. All of the data points have been normalised by the equivalent value in the experimental equal admission, peak efficiency case. A direct comparison can be made between the current CFD results and the right-most data points (circled) in both

the experimental data and the previous CFD results of Copeland *et al* since these represent exactly the same partial admission condition modelled in this study.

From Figure 7 it seems that the current CFD model predicts the normalised efficiency of the turbine to be around 22% higher than was measured on the experimental case, although the current computational analysis does fit quite well with the trend predicted by the CFD model of Copeland *et al* (2010). Given the fact that mesh density seemed to impart little influence on the prediction of turbine performance in the single passage analysis, it is not surprising that the current CFD analysis aligns well with the model of Copeland *et al* despite the current mesh being an order of magnitude larger. It is worthwhile to note however, that the prediction of the ratio of pressures between the two limbs matches the experimental values more closely in the current case compared to the previous analysis of Copeland *et al*. The current computational analysis predicts the ratio of pressures between the inner limb and the outer limb to be 1.777, this compares well to the experimentally measured value of 1.745, the CFD analysis of Copeland *et al* predicted 1.864.

Although it was not shown that this mesh should necessarily give a grid independent solution, the high spatial refinement may be expected to ensure that the flow field is predicted with a reasonable degree of accuracy. Unfortunately no experimental data exists to enable validation of the predicted flow field. From the single passage analysis however the current mesh obtained a fair agreement with the experimental data in terms of turbine performance. Considering this one may assume that the performance of the turbine in the partial admission case should also be reasonably well predicted; this leads to a question of the origin of the discrepancy seen in Figure 7, which is much larger than any discrepancy in the single passage analysis.

In order to understand the incongruity between the computational and experimental results it is necessary to look at the differences between the two. The most obvious effect is that of windage on the back face of the rotor wheel. Using a correlation given by Japikse and Baines (1994) an approximate value of torque exerted on the rotor wheel due to windage was calculated. In this case it was found that windage would have less than a 0.5% effect on the shaft power output of the turbine. Clearly this cannot account for the large disparity between the computational and experimental results.

Perhaps a more significant effect is in the calculation of turbine torque. Using the maximum experimental uncertainty in torque measurement given by Copeland (2009) this leads to a discrepancy in the measured power output of the turbine of less than 1%, this value however, is based upon the measurement of a constant torque. The CFD model predicts a time dependant cyclic torque curve with a period equivalent to one rotor blade pitch of rotation (30 degrees) with amplitude of 10% of the mean average torque. This is due to a momentary large

torque experienced by each blade as it moves from the stagnant region of the volute to the flowing region, where a jet of fluid from the first nozzle passage in the flowing sector impinges on rotor blade. This effect was also evident in the analysis of Copeland *et al.* (2010). In the experimental case a single torque measurement was taken from the dynamometer which was assumed to be the average turbine torque: it is not clear that this value will correspond to the mean average value used to calculate the turbine efficiency in the CFD analysis. Although this is not necessarily an error it does introduce an uncertainty of up to $\pm 10\%$ in the predicted torque. Unfortunately, to resolve this cyclic torque behaviour in the experimental case is unfeasible due to the very high frequency nature of these pulsations, nearly 10kHz at this rotor speed. Consequently it is difficult to quantify this effect with the current experimental data set.

Figure 8 shows a closer comparison between the CFD analysis and the experimental data for the isentropic throat area, the discrepancy is on the order of 3% in this case. Again the current CFD model aligns well with the trend predicted by Copeland *et al*. but with a better prediction of the ratio of pressures between the two limbs.

4.2.2 Passage Losses

Figure 9 shows the distribution of entropy generation within the nozzle and rotor wheel for the partial admission case. The results are plotted against the angular position to show how the loss distribution changes around the periphery of the rotor wheel. This figure represents a snapshot of the loss distribution in the turbine taken at a single instance in time. In the stator this gives a resolution of 15 degrees since there are 24 nozzle vanes, however in the rotor there are 12 blade passages giving a resolution of 30 degrees. This is equivalent to calculating the loss distribution in a single rotor blade passage at 12 instances in time, each 30 degrees of rotation apart. The normalisation value was taken as the total entropy production in the nozzle and rotor for 1 passage in the full admission, peak efficiency case (Operating point A in Figure 6).

Integration of the total entropy production in the flowing and non-flowing sections in Figure 9 reveals that the total entropy generation in the non-flowing sector of the volute is about 8% higher than that in the flowing sector. The loss in the non-flowing sector is primarily due to the dissipation of mechanical energy associated with turning the rotor wheel through the stagnant region of the volute, this must be taken from the useful work developed in the flowing section of the turbine. This sharply demonstrates why the efficiency of the double entry turbine drops so much under the partial admission condition and suggests that minimisation of energy dissipation in the non-flowing sector could have a significant impact on the performance of this double entry turbine under partial admission conditions. However, significant entropy generation in the non-flowing sector is

not the only adverse effect of partial admission. Although the conditions driving the turbine in the flowing sector of the volute are very near to those driving the turbine at peak efficiency, it is clear that the loss distribution is very different from the equivalent full admission case.

Figure 10 shows a breakdown of the losses at 4 different operating points, including the full admission, peak efficiency case (A), and three points throughout the flowing sector of the volute in the partial admission case (D, E and F). Operating point A is indicated in Figure 6, points D, E and F can be seen on Figure 9. The same normalisation value was used in Figure 9 and Figure 10.

At the start of the flowing section (operating point F in Figure 9 and Figure 10) there is a large contribution from the Pressure Side and Suction Side Passage sections (*PS Passage* and *SS Passage*) and also the *Interspace* region. This is a clear departure from the full admission peak efficiency case which sees very little entropy generation in these areas. As the wheel rotates, moving from operating point F to E and then to D, the entropy production in these areas diminishes, moving towards a loss distribution which resembles more closely that of the full admission peak efficiency case although it does not seem to reach full development before returning to the non-flowing sector. Even at the end of the flowing sector (operating point D) the passage losses are 17% higher than those in the full admission case although the breakdown of losses is similar.

In the non-flowing entry the loss distribution shows an even larger departure from any full admission case for the whole section, (see Figure 9) this is due to the turbine wheel acting in a whole different regime. In the non-flowing entry the turbine is acting more like a very inefficient compressor as it is being driven through the flow instead of extracting useful work from the fluid.

Figure 11 shows a contour plot of entropy generation within the volute, nozzle and rotor wheel at 50% of blade span. The normalisation value was chosen based on optimum visualisation of regions of high entropy production. This plot can be used to explain some of the features seen in Figure 9 although in order to examine the flow field in the partial admission case more fully it is also useful to survey the vorticity. Vorticity is a useful concept because in one sense it relates directly to the flow field, showing the local rate of rotation of the fluid, but it also acts as an indication to the creation of turbulence. Ultimately turbulence will lead to the dissipation of mechanical energy, which is the primary interest of this study. Figure 12 shows contours of vorticity magnitude at 20, 50 and 80% of blade span. In this figure the constant span plots have been unwrapped such that the whole 360 degrees of the nozzle ring and turbine wheel have been represented in a linear blade to blade plot, the flowing and non-flowing entries have been shown. Although most of the following commentary

refers to the 50% span plot it is clear that many of these features are also directly evident in the plots at 20% and 80% of blade span.

On examination of the flow field in the non-flowing section of the rotor wheel it becomes clear that there are several major effects causing loss generation. In the first nozzle passage of the non-flowing section (Feature 1 in Figure 12) there is an intense region of vorticity. This is due to leakage from the adjoining higher pressure limb through a gap between the volute tongue and the connecting stator blade leading to a region of circulating flow within the nozzle passage. Evidence of this effect is also visible in Figure 11 which shows significant entropy generation in the first nozzle of the non-flowing section (Feature 1), and in Figure 9 which shows a spike in the entropy generation within the stator at the start of the non-flowing section. Although this seems a small effect, Figure 9 shows the generation of entropy in this area to be a significant contributor to the overall entropy generation within the turbine. A similar phenomenon is observed in the last nozzle of the non-flowing sector.

Downstream of this nozzle blade there is a shear layer where the high velocity fluid from the adjoining limb mixes with the lower velocity fluid in the non-flowing region (Feature 2 in Figure 11 and Figure 12). This effect is perhaps the most significant contribution to the high entropy generation seen in the *Interspace* region in the non-flowing section in Figure 9 and seems to be one of the most significant areas of mechanical energy dissipation in the whole turbine.

Referring to Figure 9, the next most significant loss in the non-flowing section comes from within the blade passage (*PS Passage* and *SS Passage*). The contribution of these areas is seen to increase as the rotor wheel moves through the non-flowing section (moving in the direction of rotation in Figure 9). This can be primarily attributed to the development of strong vortices on the leading and trailing edges of the rotor blade (Features 3 and 4 in Figure 11 and Figure 12). As the rotor passage first enters the non-flowing section of the volute it is evident that the fluid within the passage has considerable momentum and does not stop flowing instantaneously, this helps to delay the development of these vortices however, by the time the rotor passage has reached the 4^{th} or 5^{th} nozzle in the non-flowing section, the flow within the rotor passage has slowed considerably. Referring to the vortex on the leading edge of the blade (Feature 3), as the rotor continues to turn, the slow moving fluid in the interspace region will impinge on the suction surface of the blade where it is then accelerated around the leading edge. The fluid then separates from the pressure surface leading to the formation of a vortex on the leading edge of the blade which grows rapidly to span across the whole rotor passage from the pressure surface to the suction surface. This creates a significant blockage to the flow entering the passage. This vortex is

maintained as the rotor wheel moves through the non-flowing section and right into the flowing sector of the turbine. A similar mechanism is observed in the creation of a vortex at the trailing edge of the blade (Feature 4).

Moving from the non-flowing region back to the flowing region another shear layer is formed where the high velocity flow meets the neighbouring stagnant fluid (Feature 5 in Figure 11 and Figure 12). Although this does directly cause a certain amount of entropy generation (see Figure 11), this is not to the same extent as the shear layer formed moving from the flowing region into the non-flowing region (Feature 2 in Figure 11) however, its effect is wider reaching. As the rotor wheel moves into the flowing section of the volute the vorticity generated in this shear layer is convected into the blade passage where it meets with the high vorticity region on the leading edge of the blade, carried through from the non-flowing section, associated with Feature 3 in Figure 12. This creates a region of significant vorticity at the entrance to the turbine passage, which has a large impact on the flow entering the blade passage. The vortex on the trailing edge of the blade, associated with Feature 4 in Figure 12, creates a further blockage at the exit of the first rotor passage causing more disruption to the flow. As the turbine wheel rotates through the flowing section these vortical regions are convected with the flow. The trailing edge vortex only imparts a noticeable effect on the flow structure in the first passage of the non-flowing section however, even up to 90 degrees of rotor rotation into the flowing section the vortices originally formed at the entrance to the rotor passage are still having an evident effect on the flow field, see Feature 6 in Figure 11 and Figure 12 which show evidence of the remnant vortical structure in the turbine passage at this point.

Throughout the whole period of rotor rotation in this section it seems that the rotor passage does not reach a fully developed state, although it is definitely moving towards this. The combination of the shear layer at the meeting between the flowing and non-flowing sections and the vortices formed on the leading and trailing edges of the blade throughout the non-flowing section have a definite detrimental effect on the development of the flow within the turbine passage in the flowing section. This suggests that the flow within the rotor wheel in the partial admission case is fully unsteady: Copeland *et al* (2010) also made this conclusion in their CFD analysis of the partial admission condition.

5. Conclusions

A detailed computational study was undertaken in order to investigate the distribution of losses inside a double entry turbine under conditions of both full and partial admission. Each rotor passage was divided into 7

different control volumes: each nozzle blade was taken as a single control volume. The concept of entropy generation rate was used to calculate the magnitude of loss within each control volume.

Ten conditions of full admission were simulated at 90% speed using a single passage turbine model. The prediction of turbine efficiency by the single passage model exhibited a reasonable agreement with the experimental data, the peak efficiency was predicted within 5% of the measured value. The CFD model did predict a steeper decline in efficiency with increasing velocity ratio than was measured on the experiment, leading to larger discrepancies in the lower power region of the performance curve. The prediction of mass flow by the CFD analysis was very good, being within 3% of the measured experimental values presented by Copeland (2009) for the whole range of data and significantly closer at conditions of higher power.

For the peak efficiency case the main area of loss generation was associated with the tip leakage loss. This is a parameter that turbine designers already endeavour to minimise. Although further reduction in the tip gap clearance may be possible, especially on the experimental turbine used in this study, this is can be difficult to achieve on a production exhaust turbocharger whilst maintaining the necessary mechanical integrity of the turbine. For the higher velocity ratio conditions (lower pressure ratio) the most significant loss was found to result from a large separation on the pressure side of the blade due to a highly negative incidence angle in this case. The opposite was true of the high pressure ratio (low velocity ratio) case which saw a positive incidence angle, this led to a separation on the suction side of the blade though not as severe.

In order to allow simulation of the partial admission condition a full turbine model was created incorporating the volute, 24 nozzle passages, 12 rotor passages and an exit duct. This contained over 14 million mesh nodes in total. A single partial admission condition was simulated, the boundary values were taken directly from experimental measurements. Good agreement was found with the experimental results in the prediction of the isentropic flow area. This result aligned well with the previous computational results of Copeland *et al* (2010). The prediction of turbine efficiency did not match the experimental data as closely but again did align well with the CFD analyses of Copeland *et al*. Although some difference would be expected between the computational and experimental results, further research would be required to fully account for this discrepancy.

An entropy audit was carried out using the same control volumes in each blade passage as those defined for the full admission case. This made it possible to compare the distribution of losses within the turbine in the full and partial admission cases and to identify the main areas leading to increased losses in the partial admission case. It was found that the generation of entropy in the non-flowing sector of the turbine was similar in magnitude to the generation of entropy in the flowing sector of the turbine. This will have a significant effect on

the turbine efficiency since the power associated with generating this entropy in the non-flowing section will be taken from the useful shaft work developed in the flowing section of the turbine. Minimisation of these losses could have a significant effect on the turbine performance, even if the efficiency of the turbine in the flowing section of the volute were compromised. The loss distribution in the partial admission case was very different to that seen in any full admission case for both the flowing and non-flowing sectors.

An analysis of the flow field within the partially admitted turbine was undertaken in order to identify the sources of these losses. One of the most significant areas of entropy generation in the whole turbine was associated with the shear layer formed between the flowing and the non-flowing regions. This was evident at both tongues although the effect was most severe where the turbine wheel moves from the flowing section into the non-flowing section. By itself this area represents a meaningful portion of the overall entropy generation within the turbine system. This implies that the turbine nozzle ring should be an area of concern in future turbocharger design, for example by experimentation with different nozzle-rotor gaps or different nozzle stagger angles.

Another important area of entropy generation in the non-flowing section is at the leading and trailing edges of the blade pressure surface where vortices are formed as the rotor wheel is driven through the stagnant fluid. Not only does the shearing of the fluid, associated with these vortical structures, cause a significant amount of entropy generation but they also have a wider effect as they are carried through to the flowing section of the turbine. Here they impact on the passage flow structure, blocking the flow entering and exiting the passage.

As the rotor moves through the flowing region these vortical structures are convected through the passage. It is evident that the passage flow is moving towards a fully developed state although it is clear that this is not reached before the rotor wheel moves back to the non-flowing section. This shows that the rotor wheel in a partially admitted double entry turbine is operating in a fully unsteady regime, even though the conditions driving the turbine are time invariant.

Although this work has served to increase the understanding of the partially admitted double entry turbine it could be extended to look at different conditions of unequal admission. The ultimate aim however, would be to apply the techniques used in this study to a computational analysis of a double entry turbine under pulsed operation.

6. Nomenclature

k	Thermal Conductivity	$[W/m.K]$
$\dot{Q}$	Rate of Heat Input	$[W/kg]$
RP	Ratio of Pressures between the Inner and Outer limbs	
s	Specific Entropy	$[J/kg.K]$
T	Temperature	[K]
t	Time	[s]
δ_{ij}	Identity Matrix	
λ	Bulk Visocity	[Pa.s]
μ	Dynamic Viscosity	[Pa.s]
ρ	Density	$[kg/m^3]$
σ	Entropy Generation Rate per unit Volume	$[W/K.m^3]$
τ_{ij}	Shear Stress Tensor	[Pa]

6.1 Subscript

i, j	Cartesian Components
t	Turbulence quantity

6.2 Superscript

‘	Fluctuating Component
$\dot{}$	Derivative w.r.t time
$\bar{}$	Average component

7. References

Baines, N. C. et al., 2003, Axial and Radial Turbines, Concepts ETI Inc., ISBN 0933283121.

Benson, R., 1974, Nonsteady flow in a turbocharger nozzleless radial gas turbine, SAE National Combined Farm, Construction & Industrial Machinery and Powerplant Meetings, Sep 9-12 1974, SAE Paper 740739.

Benson, R.S., Scrimshaw, K.H., 1965. An experimental investigation of non-steady flow in a radial gas turbine, IMechE Conference Proceedings 1964-1970 vols 180, 180:74-85

Copeland, C. D., 2009, The Evaluation of Steady and Pulsating Flow Performance of a Double-entry Turbocharger Turbine, PhD Thesis, Imperial College London.

Copeland, C. D., Martinez-Botas, R. F., Seiler, M., 2008. Unsteady performance of a double entry turbocharger turbine with a comparison to steady flow conditions, Proc ASME Turbo Expo 2008 GT2008-50827. pp. 1579-1588.

Copeland, C. D., Martinez-Botas, R. F., Seiler, M., 2011. Comparison between steady and unsteady double-entry turbine performance using the quasi-steady assumption. J. Turbomachinery, July 2011, 133(3), in press.

Copeland, C. D., Newton, P., Martinez-Botas, R. F., Seiler, M., 2010. Unequal Admission in a Double-Entry Turbocharger Turbine. Proc ASME Turbo Expo 2010 GT2010-22212

Denton, J.D., 1993. The 1993 IGTI Scholar Lecture: Loss Mechanisms in Turbomachines. Journal of Turbomachinery, 115(4), pp.621-657.

Greitzer, E., Tan, C., Graf, M., 2004, Internal flow: concepts and applications, Cambridge University Press, ISBN 0521343933

Japiske, D., Baines, N. C., 1994. Introduction to Turbomachinery, Concepts ETI Inc., ISBN 0-933283-10-5.

Kock, F., Herwig, H., 2005, Entropy production calculation for turbulent shear flows and their implementation in CFD codes, International Journal of Heat and Fluid Flow, 26(4), pp.672-680

Mizumachi, N., Yoshiki, H., Endoh, T., 1979, Study on performance of radial turbine under unsteady flow conditions, Report of the Institute of Industrial Science the University of Tokyo 28(1).

Moore, J., Moore, J. G., 1983a, Entropy production rates from viscous flow calculations part i - a turbulent boundary layer flow., Proc ASME International Gas Turbine Conference and Expo 1983 83-GT-70. Phoenix, AZ, USA

Moore, J., Moore, J.G., 1983b, Entropy production rates from viscous flow calculations part ii - flow in a rectangular elbow. In Proc ASME International Gas Turbine Conference and Expo 1983 83-GT-71. Phoenix, AZ, USA

Pischinger, F., Wunsche, A., 1977, The characteristic behavior of radial turbines and its influence on the turbocharging process, Proc International Congress on Combustion Engines 1977, Tokyo, Japan.

Pullan, G., Denton, J., Curtis, E., 2005. Improving the performance of a turbine with low aspect ratio stators by aft-loading, Proc ASME Turbo Expo 2005, GT2005 -68548

Sciubba, E., 1997, Calculating entropy with CFD, ASME Mechanical Engineering, 119(10), pp.86-88.

Wallace, F.J., Adgey, J.M., Blair, G.P., 1969, Performance of Inward Radial Flow Turbines under Non-Steady Flow Conditions, Proc IMechE 1847-1982 vol 184, pp. 183-195.

Wallace, F.J., Blair, G.P., 1965, Pulsating-flow performance of inward radial-flow turbines, Proc ASME Meeting GTP-21, Feb 28-Mar 4 1965

Wallace, F.J., Miles, J., 1970, Performance of Inward Radial Flow Turbines Under Unsteady Flow Conditions with Full and Partial Admission, Proc IMechE 1847-1982 vol 185, 185 77/71, pp1091-1106.

Watson, N., Janota, M. S., 1982. Turbocharging the Internal Combustion Engine, The MacMillan Press ltd., ISBN 0 333 24290 4, pp275.

8. Figures

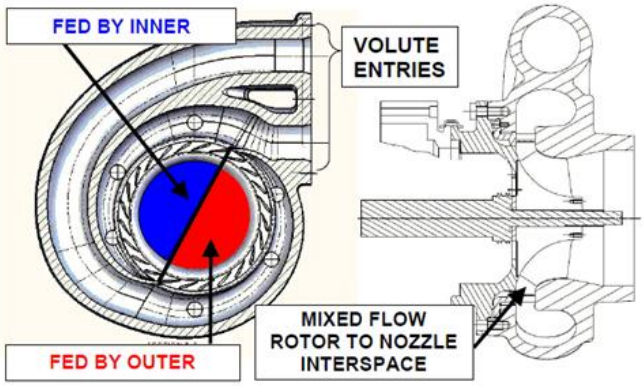

Figure 1. Double entry volute configuration

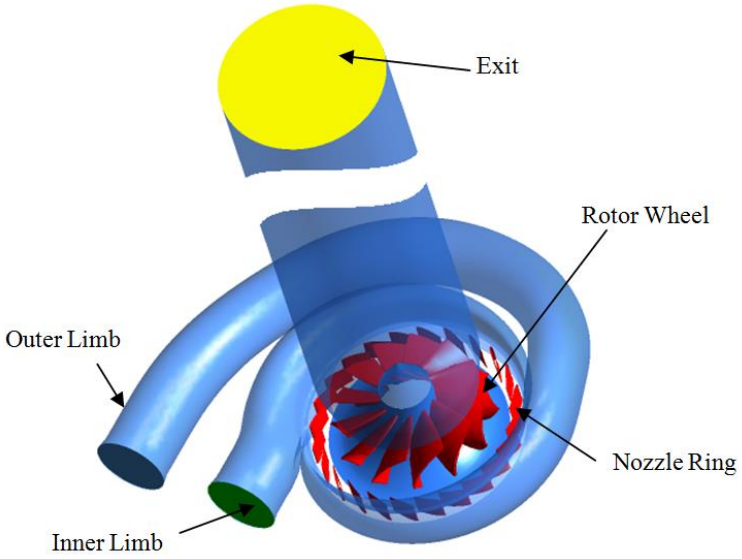

Figure 2. Full turbine domain for the partial admission case with the inner (flowing) and outer (non-flowing) limbs marked, the rotor and nozzle blades can be seen in red and have also been marked along with the exit plane.

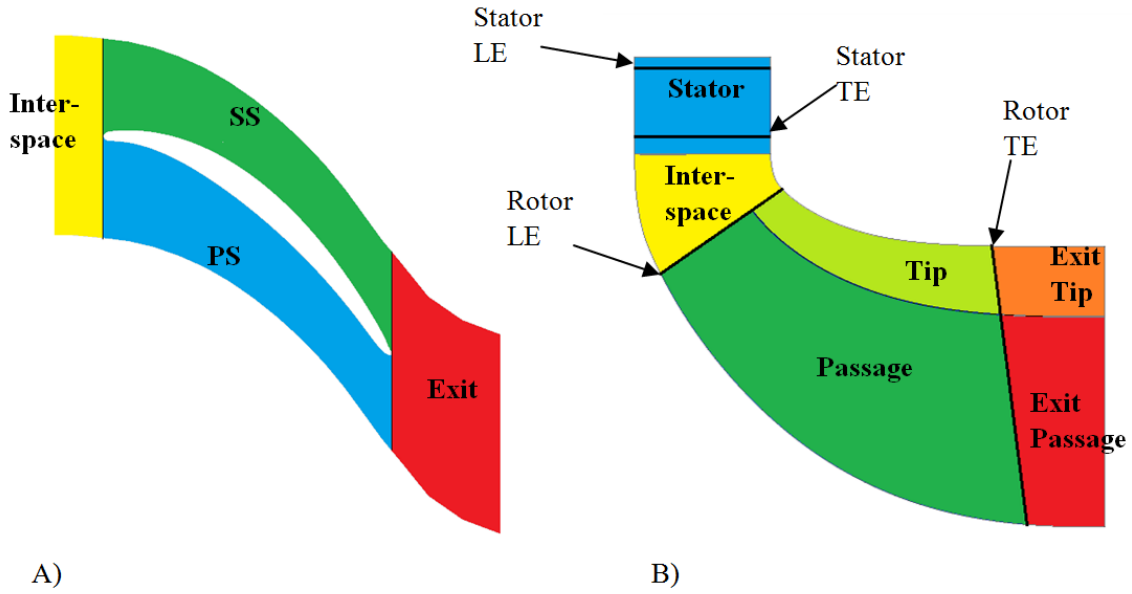

Figure 3 A) Division of rotor blade passage in the blade-to-blade orientation, the Suction Side (SS), Pressure Side (PS) and Exit areas are further divided into Passage and Tip areas. B) Division of the rotor and stator domains in the meridional sense, the leading and trailing edges of the rotor and stator blades have been marked. The tip area (Tip and Exit Tip) incorporate everything above 75% of span.

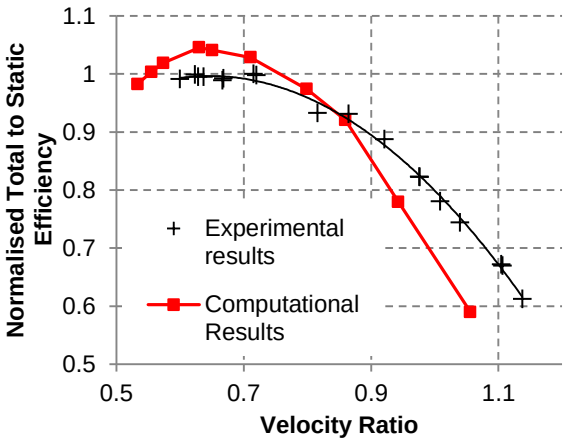

Figure 4. Comparison of CFD data with experimental data for full admission efficiency

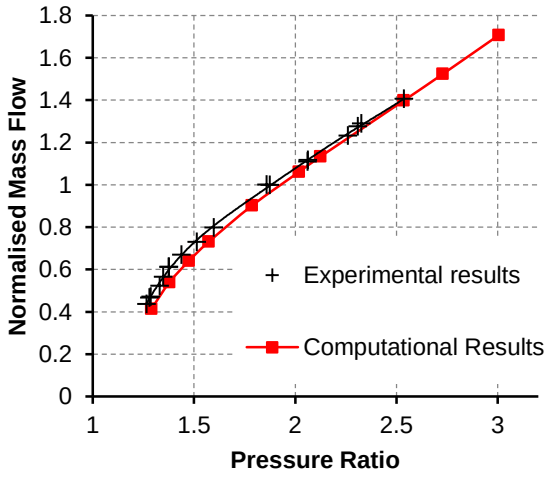

Figure 5. Comparison of CFD data with experimental data for full admission mass flow rate

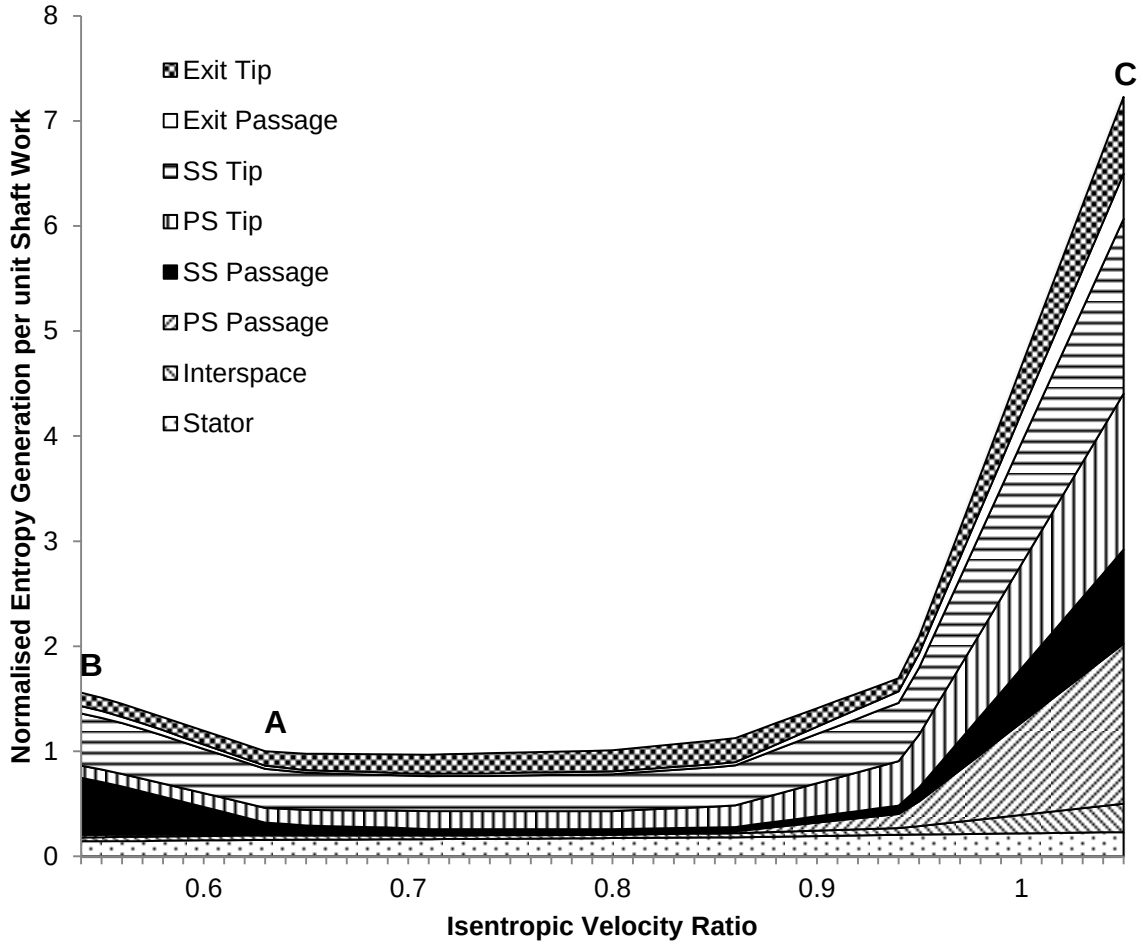

Figure 6. Division of losses in the turbine system for a single passage model, relative to the shaft work of the turbine. Operating point A shows the peak efficiency case (pressure ratio 2.1, velocity ratio 0.63), this also corresponds to point A in Figure 10, operating point B shows the highest pressure ratio case (pressure ratio 3.0, velocity ratio 0.53) and C shows the lowest pressure ratio case (pressure ratio 1.3, velocity ratio 1.05)

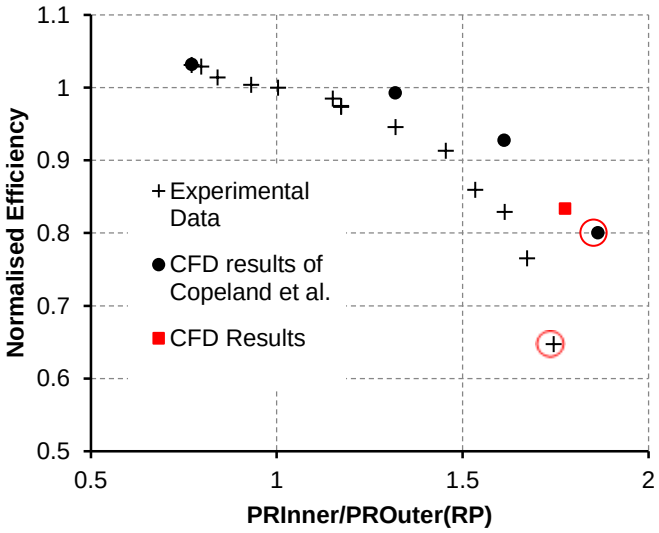

Figure 7. Comparison of Partial Admission CFD Efficiency with Experimental Data and the previous results of Copeland et al. (2010), the results for direct comparison with the current CFD case have been circled.

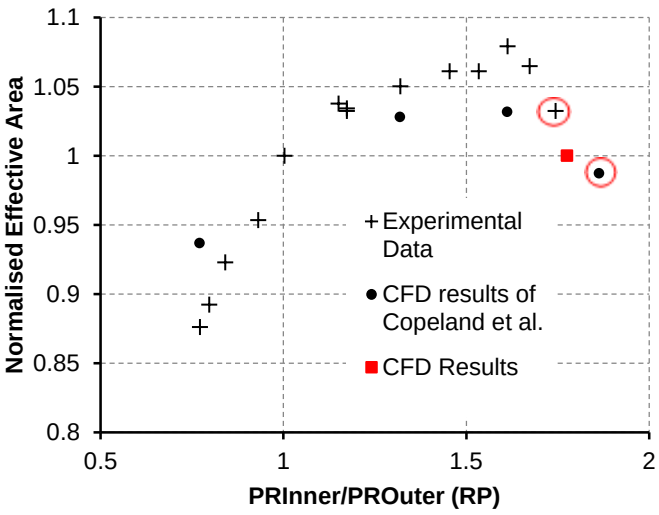

Figure 8. Comparison of Partial Admission CFD Effective Area with Experimental Data and the previous computational data of Copeland et al. (2010), the results for direct comparison with the current CFD case have been circled. This figure shows only the effective area calculated for the inner limb, in the experimental data and the CFD results of Copeland et al. the pressure ratio across the inner limb was held at around 2.0 whilst

the ratio of inlet pressures was varied by adjusting the pressure ratio across the outer limb, in the partial admission case the outer limb was closed such that no mass could flow.

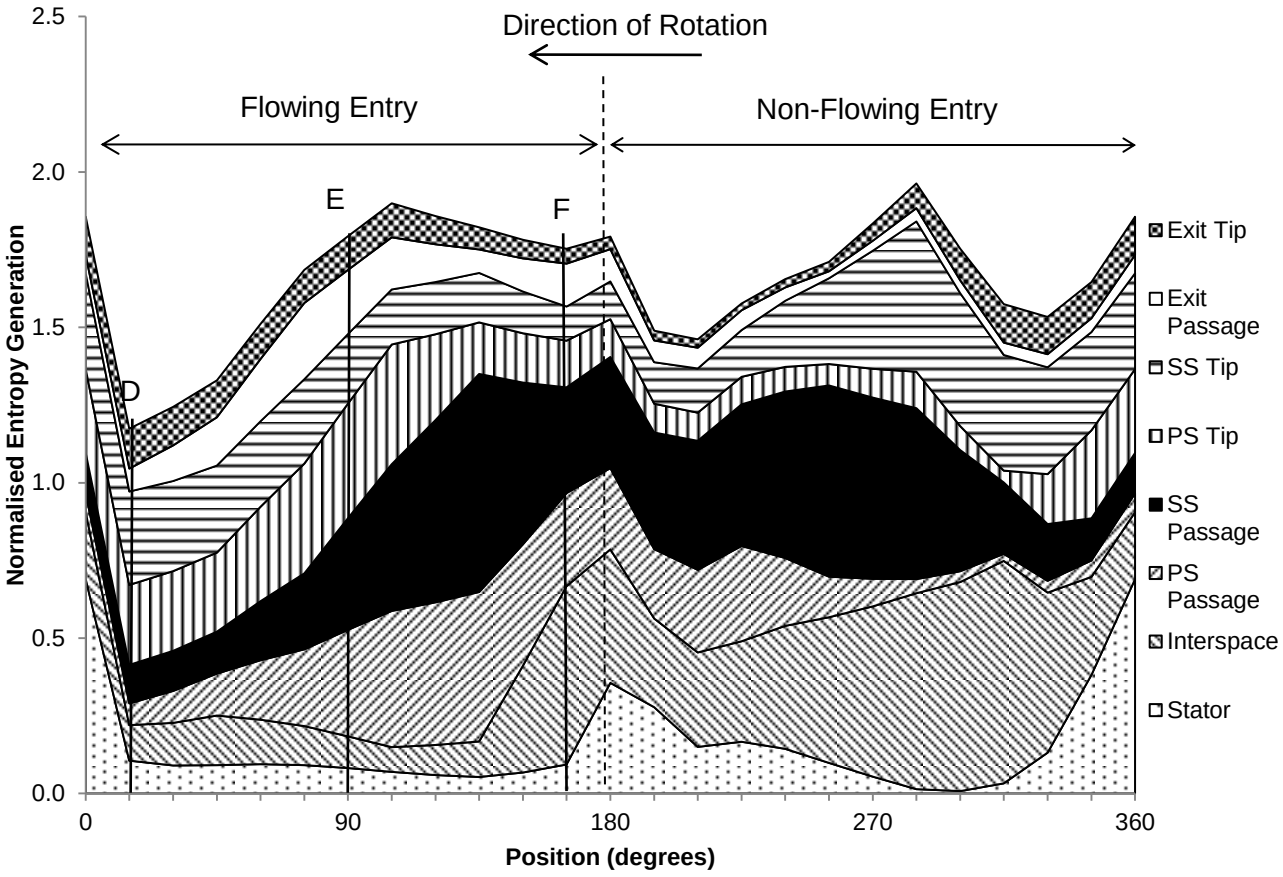

Figure 9. Distribution of Entropy Generation against position in the Partial Admission case at a single instance in time, the sections corresponding to the flowing and non-flowing sections have been marked, the rotation direction is shown. Operating points D, E and F relate to Figure 10. The angular position of the turbine can be seen physically in Figure 11.

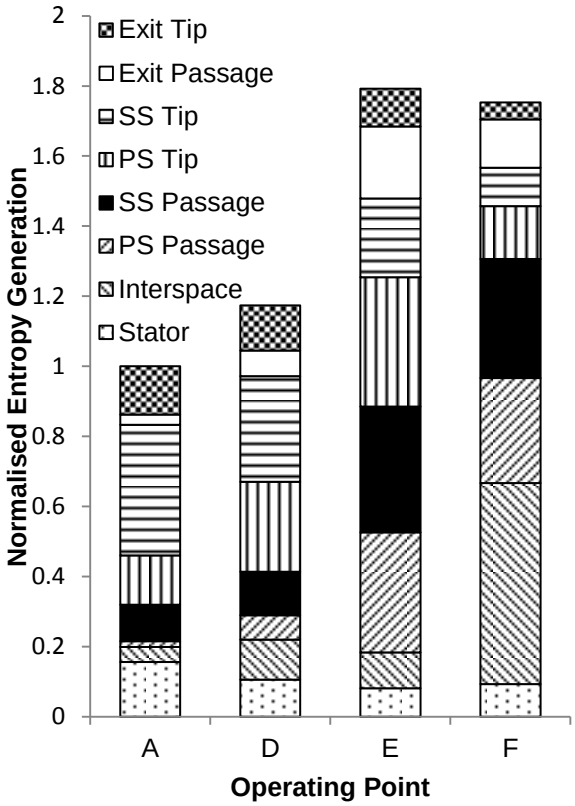

Figure 10. Distribution of entropy generation within a single turbine passage at different operating points of the turbine: including the full admission peak efficiency case (A, see Figure 6) and at 3 points through the flowing sector in the partial admission case (D, E & F, see Figure 9).

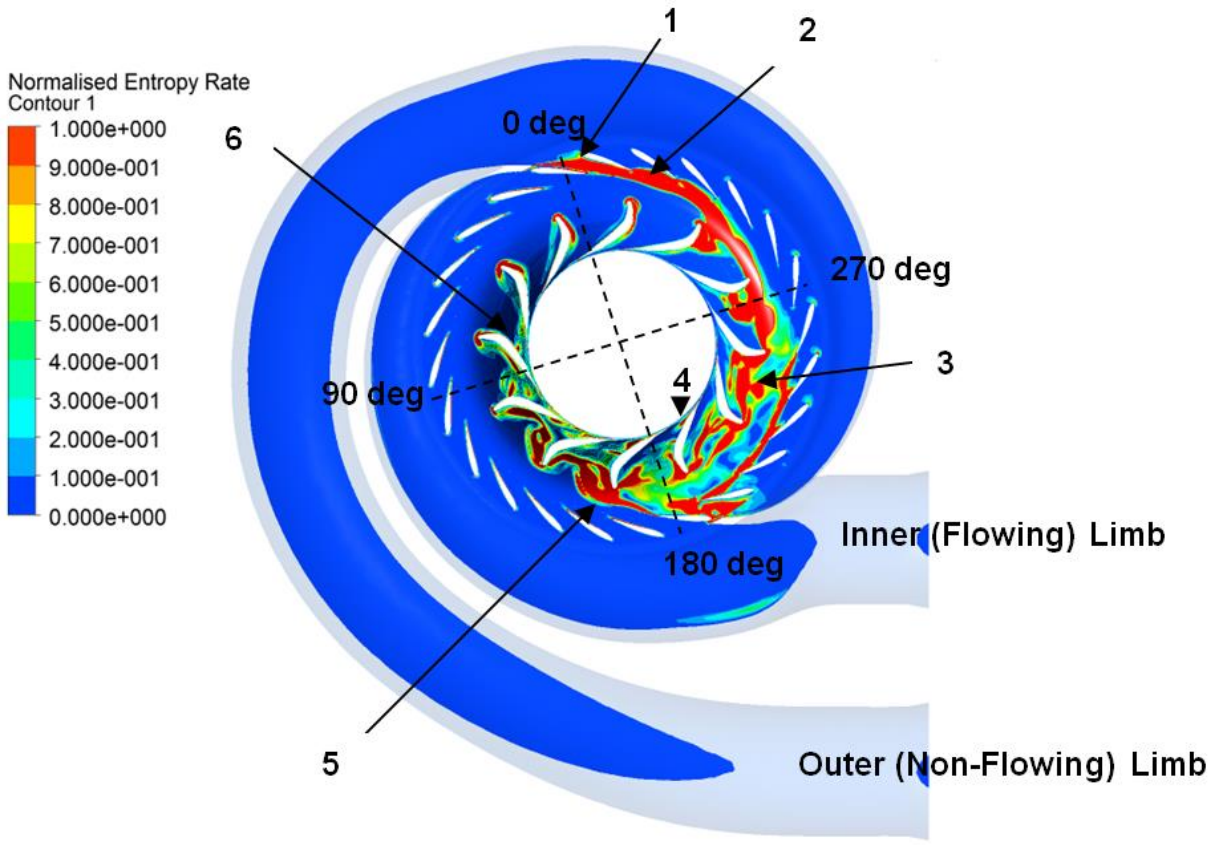

Figure 11. Contour of Normalised Entropy Generation Rate at 50% span, the numbers correspond to the same features seen in Figure 12, the angles correspond to those on Figure 9. The inner (flowing) and outer (non-flowing) limbs have been marked.

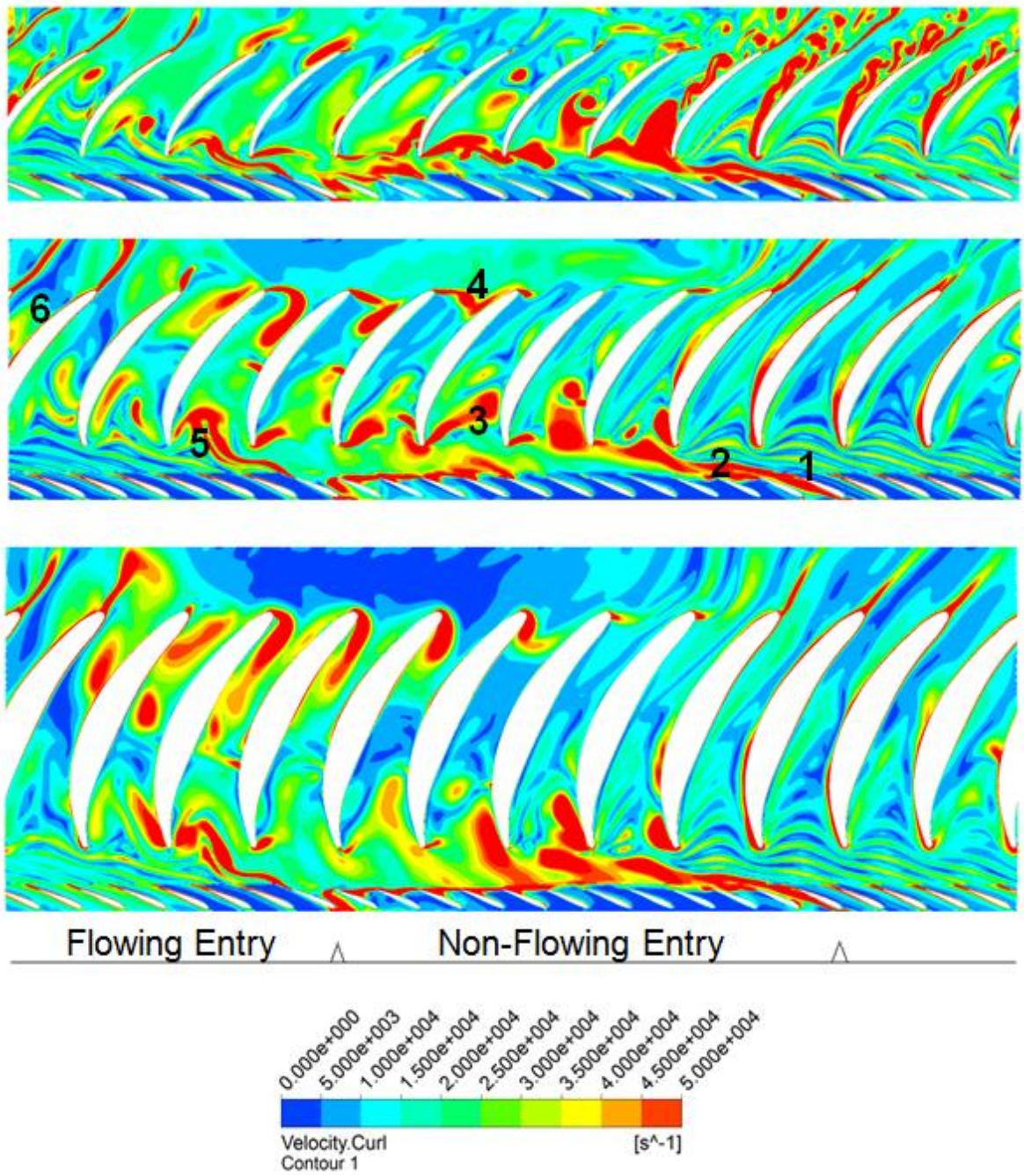

Figure 12. Contours of Vorticity Magnitude in the blade to blade plane at 20, 50 and 80% of blade span with the flowing and non-flowing entries marked. The figure has been annotated to show several features of the flow, also shown in Figure 11.

9. Tables

Table 1. Single Passage Model Settings

Analysis type	Steady state
Inlet	Total Pressure and Static Temperature. Flow direction assuming a free vortex flow with a swirl coefficient of 0.9 (Japiske & N C Baines 1994)
Outlet	Area averaged static pressure
Nozzle Rotor Interface	Stage Interface
Walls	Smooth, adiabatic
Turbulence Model	k-ε with scalable wall functions

Table 2. Partial Admission Model Settings

Analysis type	Transient, 1 Degree of Rotor rotation per time-step
Inner Limb Inlet	Total Pressure and Total Temperature, flow direction normal to volute inlet plane
Outer Limb Inlet	Wall boundary condition
Outlet	Area averaged static pressure
Nozzle Rotor Interface	Transient rotor stator interface
Walls	Smooth, adiabatic
Turbulence Model	k-ε with scalable wall functions